ECCOMAS Congress 2016
VII European Congress on Computational Methods in Applied Sciences and Engineering
M. Papadrakakis, V. Papadopoulos, G. Stefanou, V. Plevris (eds.)
Crete Island, Greece, 5–10 June 2016

DATA ASSIMILATION USING MRI DATA

Geir Nævdal[1], **Ove Sævareid**[1], **and Rolf J. Lorentzen**[1]

[1]International Research Institute of Stavanger (IRIS)
Thormøhlensgate 55, N-5008 Bergen, Norway
e-mail: {gen,osae,rjl}@iris.no

Keywords: Contrast enhanced dynamic MRI data, multi-compartment porous media flow modelling, data assimilation, ensemble Kalman filter

Abstract. *Contrast enhanced dynamic MRI data is important for classifying anomalies in tissue and blood circulation, e.g. tumors, stokes, kidney failure. The resulting sequence of images providing spatial-temporal representation of contrast agent concentration must be given meaningful clinical interpretation. Current processing typically relies on localized strategies, where the images are analyzed voxel by voxel. The consensus seems to be that taking direct advantage of the global structure of the images potentially will allow for more accurate and robust interpretations.*

Based on a workflow that has been extensively studied within both petroleum and ground water research, the current paper combines explicit porous media flow modelling and state of the art data assimilation. Starting from a multi-compartment global flow model, we explore MRI interpretation via synthetic cases where model generated images are used as input to a parameter identification algorithm based on ensemble based data assimilation like the ensemble Kalman filter (EnKF).

From reasonable assumptions, the procedure demonstrates ability to identify relevant model parameters for two synthetic cases.

This study indicates that flow based assimilation of MRI data is viable and that it might provide valuable supplementing insight compared to state of the art. Regularizations are made on a firm statistical basis, eliminating the need for ad hoc parameters, and leading to estimates that are rigorous in terms of error thresholds. A priori knowledge can easily be incorporated in the procedure. The flow model allows explicit representation of basic material properties, and adds regularization to the procedure by enforcing globally consistent flow fields.

1 INTRODUCTION

Magnetic resonance imaging (MRI) enhanced by an injected contrast agent is a useful tool for characterizing the blood flow in organs like brain or kidney. The procedure provides a high resolution spatial-temporal representation of *contrast agent concentration* (CAC) over the object considered, and the aim of the subsequent interpretation is to extract clinically useful parameters. Assessment of brain blood supply relies on concepts like *cerebral blood volume* (CBV), *cerebral blood flow* (CBF), and *mean transit time* (MTT) of the blood flow.

The traditional parameter identification approach, see [1] for a detailed review, relates the observed average CAC across a *volume of interest* (VOI) to the CAC of the incoming (arterial) blood stream by the convolution

$$C_{\text{VOI}}(t) = (C_{\text{arterial}} * k)(t) \quad , \tag{1}$$

where the response function $k(t)$ is the flow-scaled residual and can be determined by explicit deconvolution or alternatively from various ad-hoc procedures. Given $k(t)$, the following estimates are available

$$\text{CBF} = \frac{\max\left(k(t)\right)}{\rho_{\text{VOI}}} \ , \quad \text{MTT} = \frac{\int_0^\infty k(\tau)d\tau}{\max\left(k(t)\right)} \ , \quad \text{CBV} = \text{MTT} \cdot \text{CBF} \tag{2}$$

where ρ_{VOI} denotes the mean density of the tissue constituting the VOI.

The significance of CBF is to identify the amount of blood that is actually feeding the local tissue. Applying the above approach voxel-wise based on modern high resolution imaging has certain limitations. It can be difficult to isolate the relevant arterial influx, and the observed CAC for the voxel will typically represent a superposition of blood in transit in the arterial and/or venular system as well as blood relevant to the local CBF. Voxel-wise temporal deconvolution also neglects the potential useful spatial structure of the observations.

These challenges are addressed by [2], where a systematic approach is formulated in terms of discrete spatial-temporal conservation relations for the CAC. The procedure can readily be extended to so-called multi-compartment models, where the total flowing volume of each voxel is partitioned into a set of distinct but interacting compartments. Each compartment type connects globally throughout the voxel-lattice thus constituting a set of interacting flow networks. Connection coefficients governing the flow between voxels and exchange between compartments can then in principle be identified from the evolving CAC distribution.

The current work is directly inspired by Sourbron [2], and in particular his section IV-D where he formulates a two-compartment model for "blood flow and perfusion". While Sourbron identifies the flow pattern by solving for a set of abstract connection coefficients, our approach is based on explicit physical modelling and identification of basic physical properties. We strongly believe that maintaining complete physical consistency throughout our computations may contribute important regularization to the problem.

It is natural to start to investigate if one can identify the volumes for the different compartments within a voxel by combining the use of a physical model for the flow of the contrast agent through some live tissue with the information obtained from a high resolution spatial-temporal representation of the CAC obtained from MRI. A natural approach is to use data assimilation methodology developed for characterization of the properties of a porous medium (e.g. flow in an oil reservoir or a hydrological model) developed over the last decades. A common approach is to use ensemble based methods, like the ensemble Kalman filter (EnKF) [3] for solving such problems (see e.g. [4], [5]). Alternatively, the Adaptive Gaussian Mixture filter (AGM) [6]

may be used. This filter is a combination of the traditional EnKF and particle filters, and was developed to better represent multi-modal posterior distributions.

The ensemble based data assimilation approaches works efficiently with large scale models. The models are updated by utilizing the information obtained from an ensemble of forecast (model simulations) with the available measurements. The EnKF and its variants are suitable for updating large scale non-linear models and is applied in a range of geophysical sciences, besides reservoir models such as meteorology (e.g. [7]) and oceanography (see e.g. [8]). Ensemble based data assimilation has also been used within medicine. In [9] a synthetic study using the local ensemble transform Kalman filter for improved forecasting for glioblastoma utilizing MRI data. In the recent paper [10] it is proposed that the cancer biology community makes an effort to utilize ideas from weather forecasting to predict and evaluate tumor growth and treatment response.

2 FORWARD MODEL

We consider a two-compartment model, or - in the terminology of traditional porous media modelling - a dual porosity, dual permeability model. One porous network (index a) is considered to represent the arterial blood flow and the other (index v) models the flow in the venular system. The interaction between the two pore networks represent the capillary perfusion feeding the local tissue, and the motivation for the model formulation is that this approach allows for an accurate identification of CBF.

We consider a spatial-temporal domain with coordinates $(\vec{x}, t)$, and the model formulation is equally valid in one, two, or three spatial dimensions. Filtration velocities, $\vec{u}_i$ for the respective networks are related to pressures p_i by Darcy's law. We assume fluid of constant viscosity μ, and permeabilities K_i that are functions of spatial position. Neglecting gravity, yields the following version of the Darcy law

$$\vec{u}_i = -\mu^{-1} K_i(\vec{x}) \nabla p_i \quad , \quad i = a, v. \tag{3}$$

We make the assumption of incompressibility for both fluid and porous media. The flow will be driven via boundary conditions, and the interior source terms q_i will only represent exchange between the compartments according to

$$\nabla \cdot \vec{u}_i = q_i \quad , \quad i = a, v. \tag{4}$$

As customary for dual models, we relate the transfer terms to the pressure difference between the compartments. The parameter σ_{av} scales for arterial/venular interface area of a unit volume, and the product $K_{av} \cdot \sigma_{av}$ constitutes a dimensionless conductivity factor at each location. Thus the volumetric flux per unit volume medium can be written

$$q = -q_a = q_v = \mu^{-1} K_{av}(\vec{x}) \sigma_{av}(\vec{x})(p_a - p_v). \tag{5}$$

Substituting equation (3) into (4) and then use equation (5) to eliminate the source terms yields a coupled system of two equations where p_a and p_v are the only unknowns. Given a domain, fluid and media properties, and suitable boundary conditions, we solve for the pressures using a standard finite volume scheme on a regular lattice. Subsequently we substitute the pressures into (3) and (5) to find velocities and transfer rates respectively.

The CAC is modelled as passive (i.e. not influencing the fluid flow) scalar field that enters along inflow boundary into the arterial network, is drained trough the capillary bed into the

venular network, and eventually leaves through the outflow boundary. The fractions of voxel volume occupied by the arterial and venular networks respectively, are given by the porosities ϕ_a and ϕ_v. As for equation (4), the source terms are exclusively related to transfer between compartments and the associated CACs are denoted c_i^*

$$\phi_i(\vec{x})\frac{\partial c_i}{\partial t} + \nabla \cdot (c_i \vec{u}_i) = q_i c_i^* \quad , \quad i = a, v. \tag{6}$$

Assuming normal operating conditions, the transfer will be one-way only, directed from arterial into venular, i.e. $q \geq 0$. We assume the CAC of the fluid leaving the arterial system at a given space-time location equals the overall arterial CAC at that location. This means $c_a^* = c_a$ and by combining equations (4) and (6) for $i = a$ we have

$$\phi_a(\vec{x})\frac{\partial c_a}{\partial t} + \vec{u}_a \cdot \nabla c_a = 0. \tag{7}$$

Thus the CAC travels unchanged along the characteristics $\phi_a \vec{dx} = \vec{u}_a dt$. By tracking the curve backwards until it hits an inflow boundary and take the time delay (time of flight) into consideration, c_a for arbitrary space and time can immediately be deduced from the appropriate boundary condition.

In order to associate a time delay with the transfer between the arterial and venular system, we introduce a third porosity, $\phi_{av}(\vec{x})$, characterizing the capillary beds. This additional compartment is assumed to be "discrete" in the sense that inter-voxel connections are omitted, a simplification justified by comparing the typical voxel size with that of a capillary bed. The time delays for given location can then be expressed as ϕ_{av}/q.

For the venular compartment, the situation is slightly more involved as the local CAC c_v normally will be different from the entering CAC c_{V}^* due to flow in the venular network and we have

$$\phi_v(\vec{x})\frac{\partial c_v}{\partial t} + \vec{u}_v \cdot \nabla c_v = q\,(c_v^* - c_v). \tag{8}$$

Again we identify a family of characteristics $\phi_v \vec{dx} = \vec{u}_v dt$, but this time CAC varies along the curves according to the right hand side of equation (8). By combining the time delay for the arterial and capillary flow, we can identify c_v^* at any point in space-time. Then c_v can be found at an arbitrary location by first tracking the characteristic curve backwards in time until one hits an inflow boundary or reaches the initial time. Starting from the relevant boundary or initial value, equation (8) is integrated forward along the characteristic curve to obtain the appropriate value for c_v.

To conclude this section, we relate our model formulation to the clinical parameters CBV, CBF and MTT. The unit used for CBF in a clinical setting will typically be either [mL/min/100g] or [mL/min/100mL], where the first is multiplied with a relevant density ρ_{VOI} of unit [g/mL] to obtain the second. Thus, starting from our inter-compartment flux q of units [1/s], the conversion factor is either $60 \times 100/\rho_{\mathrm{VOI}}$ or simply 60×100. Similarly, the unit used for CBV is normally [mL/100g] or [mL/100mL] which can be obtained by multiplying to our dimensionless capillary bed porosity ϕ_{av} with conversion factors of $100/\rho_{\mathrm{VOI}}$ or 100 respectively.

For the brain, [11] estimates the CBV for grey matter to be in the range 1.8 - 3.4 [mL/100mL] and the corresponding CBF in the range 61 - 103 [mL/min/100mL]. Thus the corresponding MTT is between 1.0 and 3.3 seconds. Similar estimates for white matter give a CBV between 0.9 and 1.7 [mL/100mL] and a CBF between 9 and 37 [mL/min/100mL], leading to MTT between 1.4 and 11 seconds. For our model parameters q and ϕ_{av}, typical values will then be 0.014 [1/s] and 0.026 [-] for grey matter, and 0.0038 [1/s] and 0.013 [-] for white matter.

3 ENSEMBLE BASED METHODS FOR DATA ASSIMILATION

Data assimilation concerns the subject of combining model and observations to improve the forecasting applicability of the model. The prototype application is weather forecasting were current observations from all available sources are taken into account before a new weather forecast is prepared. In that application, the observations are primarily used to update the initial values of the system equations that need to be solved for generating a new forecast.

As mentioned in the introduction data assimilation is used within many disciplines besides meteorology and atmospheric sciences, including oceanography, hydrology (e.g. groundwater flow) and petroleum (in particular reservoir modelling). Opposed to the initial value that one faces in meteorology, in our case, we are facing uncertain parameters in describing the blood flow through an organ. This means that we are closer to the problems faced within groundwater and reservoir modelling. For these applications an ensemble based approach is most common.

The data assimilation problem can be formulated as a minimization problem for a quadratic cost function

$$J(\vec{s}) = (\vec{s} - \vec{s}_b)^T C^{-1} (\vec{s} - \vec{s}_b) + \sum_{i=0}^{n} (y_i - G_i(\vec{s}))^T R_i^{-1} (y_i - G_i(\vec{s})). \tag{9}$$

Here $\vec{s}_b$ is the initial state estimate, C is a covariance matrix for a background error, R_i are measurement error covariance matrices, G_i are observation matrices and i is a time index and n the number of time steps. In weather forecasting variational approaches is the most common approach, whereas in other applications ensemble based methods are very popular. A variational approach will require $\nabla J(\vec{s})$. The ensemble based approaches have an advantage in that they do not require the access to the code developed for solving the forward problem.

The ensemble based approaches, like the EnKF, are typically derived based on the Kalman filter [12]. The Kalman filter can be derived as a recursive solution of the least squares problem (9). It is motivated from electrical and mechanical engineering with the aim of solving the state estimation for a linear dynamic system described by a forward model

$$\vec{s}_n = F\vec{s}_{n-1} + \vec{\epsilon}_n, \tag{10}$$

and an observational model

$$\vec{y}_n = G\vec{s}_n + \vec{\eta}_n.$$

Here, $\vec{s}$ is the state vector of the system, $\vec{y}$ denote the observations of the system, $\vec{\epsilon}_n$ denotes the model noise, which is assumed to be zero mean normally distributed with covariance matrix Σ and $\vec{\eta}_n$ is the measurement noise that is normally zero mean distributed with covariance matrix C_D. The model and measurement noise is independent, and the both the model and the measurement noise at different time instances are also independent.

Kalman [12] gave the optimal solution, given observations $\vec{y}_{o,n}$ at time step n. Starting from an initial estimate $\hat{\vec{s}}_0$ with covariance matrix C_0 representing the initial uncertainty, the following recursion provides the solution:

$$\begin{aligned}
\vec{s}_n &= F\hat{\vec{s}}_{n-1}, \\
C_n &= F\hat{C}_{n-1}F^T + \Sigma, \\
\hat{\vec{s}}_n &= \vec{s}_n + K_n(\vec{y}_{o,n} - G\vec{s}_n), \\
K_n &= C_n G^T (GC_n G^T + C_D)^{-1}, \\
\hat{C}_n &= (C_n^{-1} + G^T C_D^{-1} G)^{-1}.
\end{aligned}$$

The first two equations above represent the effect of the forward model, which propagates the mean and the covariance matrix. The third equation is the update equation taking into account the observations. The matrix K_n is denoted the Kalman gain matrix. The last equation give the posterior covariance matrix $\hat{C}_n$ after taking the information form the measurement at time n into account.

The Kalman filter was derived for a linear system, but was soon generalized to non-linear systems by the extended Kalman filter. The extended Kalman filter works by performing a linearization of a non-linear system around the mean, and works well for many mildly non-linear system. However, if the non-linearities are to large it breaks down. Another issue is that the propagation of the covariance matrices is not feasible for large-scale system.

The ensemble Kalman filter was suggested by Evensen [13], and that has been found to work for large scale system, and handle non-linearity better than the extended Kalman filter. The linear forward model (10) is now replaced with the non-linear extension

$$\vec{s}_n = F(\vec{s}_{n-1}) + \vec{\epsilon}_n \tag{11}$$

where we have kept the model noise $\vec{\epsilon}_n \sim N(0, \Sigma)$. The observation equation is

$$y_n = G\vec{s}_n + \vec{\eta}_n$$

where the measurement noise is $\vec{\eta}_n \sim N(0, C_D)$.

The ensemble Kalman filter solution is obtained by using an ensemble of N model realizations $\vec{S}_n = [\vec{s}_{n,1} \dots \vec{s}_{n,N}]$ to obtain the statistics required to solve the Kalman filter equations. The initial ensemble is generated by sampling from a normal distribution. All the ensemble members are propagated through the forward model $\vec{s}_{n,i} = F(\vec{s}_{n-1,i}) + \epsilon_{n,i}$. Here n is the time index and i is the counting of the ensemble members. Forecasted values of the observations can be computed as $y_{n,i} = G\vec{s}_{n,i} + \vec{\eta}_{n,i}$. (The noise need to be added to each ensemble member to propagate the statistics correct.) The Kalman gain is now approximated by calculating the mean of the ensemble, $\bar{\vec{s}}_n = \frac{1}{N}\sum_{i=1}^{N} \vec{s}_{n,i}$. Formally, we can also calculate the covariance matrix $\bar{C}_n = \frac{1}{N-1}\sum_{i=1}^{N}(\vec{s}_{n,i} - \bar{\vec{s}}_n)(\vec{s}_{n,i} - \bar{\vec{s}}_n)^T$ and estimate the Kalman gain matrix $K_n = \bar{C}_n G^T (G\bar{C}_n G^T + C_D)^{-1}$. From this each of the ensemble members are updated as

$$\hat{\vec{s}}_{n,i} = \vec{s}_{n,i} + K_n(\vec{y}_{o,n} - \vec{y}_{n,i}). \tag{12}$$

What is presented here is a formal derivation of the Kalman filter update equation using the ensemble Kalman filter. Care needs to be taken in the implementation, and different approaches exist on how to handle this, see e.g. [3], [4], [9].

The AGM filter utilizes the same set of equations for updating of the state variables, but in addition weights are computed (and adaptively adjusted to avoid degeneracy) for each ensemble member. The weights are then used to resample the ensemble to better represent non-Gaussian behavior. For more details, see [6], [14].

In our application, the primary aim is to estimate parameters, $\vec{p}$. This can be done by extending the state vector $\vec{s}$ to the form

$$\vec{s}_e = \begin{bmatrix} \vec{s} \\ \vec{p} \end{bmatrix}.$$

In the forward step (11) the parameters are not changed, that is,

$$\vec{s}_{e,n} = F(\vec{s}_{e,n-1}) = \begin{bmatrix} F(\vec{s}_n) \\ \vec{p}_n \end{bmatrix}.$$

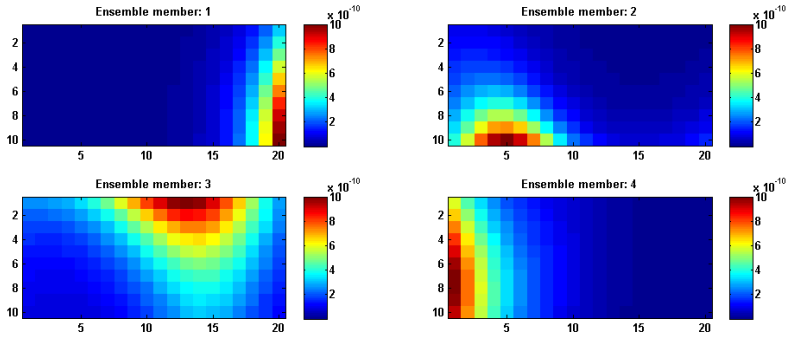

Figure 1: Four first ensemble members for permeability. The units are [m^{-2}].

However, in the update equation (12) we are now working on the extended state vector $\vec{s}_e$. As is common in reservoir engineering applications for parameter estimation we set the model noise $\vec{\epsilon}_n = 0$ in (11).

4 DETERMINING PARAMETERS IN A TWO-COMPARTMENT MODEL USING MRI DATA

We demonstrate the methodology on two examples of increasing complexity. In the first example the tissue perfusion (CBF) is estimated and in the second example the cerebral blood volume (CBV) is estimated. In both cases we consider a a square tissue field, with dimensions 10 cm $\times$ 10 cm, with resolution $n_x = 20$ and $n_y = 10$. The arterial inlet function is represented by a pulse ($C_{arterial} = 1$) lasting 4 seconds, and entering the field at the left boundary of the field. The pressure at the same boundary is 13300 Pa. At the venular compartment, the pressure boundary condition is 133 Pa at the left edge. All other edges are assumed to be sealed. The blood viscosity is $4 \cdot 10^{-3}$ Pa·s. The MRI data are simulated as the superposition of the compartment concentrations times the corresponding porosity:

$$m_{mri}(\vec{x}) = \phi_a \cdot c_a + \phi_{av} \cdot c_{av} + \phi_v \cdot c_v. \tag{13}$$

To these measurements we add independent (temporally and spatially) measurement noise of 10^{-4}.

In both the following examples the simulator is run for 60 seconds with time step of 0.6 seconds.

4.1 Estimating perfusion

In this example we assume that the permeabilities $K_i(\vec{x})$ defined in equation (3) are unknown, but we assume that the permeabilities are equal for the arterial and venular system, i.e. K_a = K_v. We further assume that the product $K_{av} \cdot \sigma_{av}$ defined in equation (5) is given by $10 \cdot K_i$. This gives one unknown parameter for each voxel in the simulated system. The ensemble members are generated as exponentials of a Gaussian randoms fields. The random fields have a spatial distribution having a Gaussian variogram [15, page 91] with practical range $\frac{10}{\sqrt{3}}$ in the x-direction and $\frac{20}{\sqrt{3}}$ in the y-direction. The fields are shifted so that the maximum value is 10^{-9}. Four realizations of the ensemble are shown on Figure 1. In this example 500 ensemble members are used. We have assumed that the porosity values for the arterial, capillary and venular systems are known. The applied fields are shown on Figure 2. The Adaptive Gaussian Mixture (AGM) filter is then applied for estimation of the true permeability field. The true field

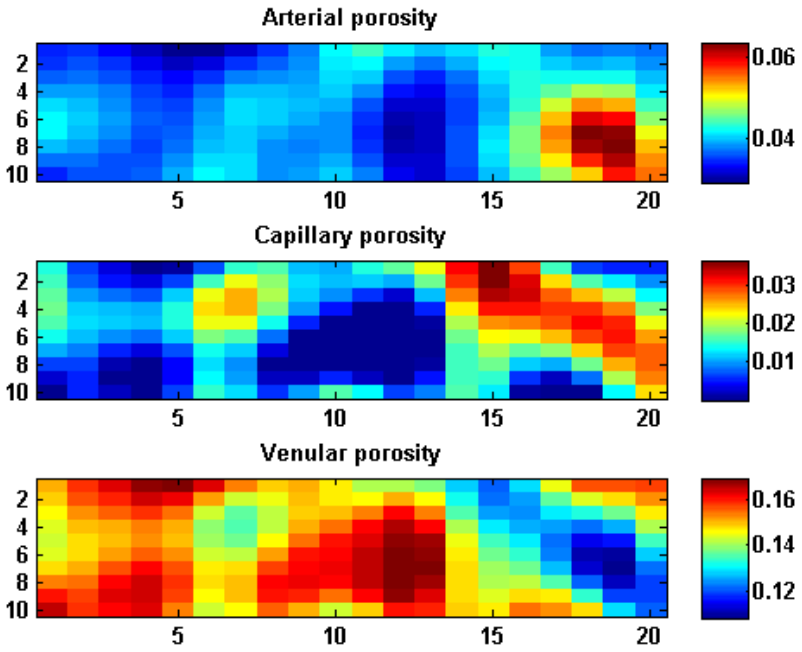

Figure 2: Porosity values for arterial, capillary and venular system.

is generated the same way as the initial ensemble. The field is updated at 24 points in time, evenly distributed within the simulation interval from 0 to 60 seconds. The true field is shown on Figure 3 (top) and the mean value of the final estimated permeability is shown on Figure 3 (bottom). As can be seen, the field is almost perfectly reconstructed. The corresponding true and estimated perfusion fields are shown on Figure 4. Finally, we show the simulated MRI data at selected points in time on Figure 5. Here we can clearly see how a rather inaccurate MRI image at the early time steps are improved as more data are assimilated.

4.2 Estimation of porosities for individual compartments

In this example we consider estimation of the porosity fields $\phi_a(\vec{x})$, $\phi_v(\vec{x})$ and $\phi_{av}(\vec{x})$ of the two-compartment model using MRI observations of the CAC as a function of time. The region we consider is the same as in the previous example, but now we have constant permeabilities $K_{av} = 2 \cdot 10^{-9} \mathrm{m}^{-2}$, $K_a = K_v = 2 \cdot 10^{-10} \mathrm{m}^{-2}$. For the porosity we generate three spatially varying fields. These fields are constructed by first generating two fields $u(\vec{x})$ and $v(\vec{x})$ a spatial distribution having a Gaussian variogram [15, page 91] with practical range $\frac{6}{\sqrt{3}}$ in the x-direction and $\frac{12}{\sqrt{3}}$ in the y-direction. Then $\phi_a(\vec{x}) = 0.003 \cdot u(\vec{x}) + 0.0375$ giving the field shown at Figure 6 (top). Then we set $\phi_v(\vec{x}) = 0.005 \cdot (-0.8 \cdot u(\vec{x}) + 0.6 \cdot v(\vec{x})) + 0.15$ and obtain the field shown in Figure 7 (top). Further we make the assumption that the $\phi_a u(\vec{x}) + \phi_v u(\vec{x}) + \phi_{av} u(\vec{x}) = 0.2$ and this defines ϕ_{av} as shown in Figure 8 (top). (Note that $\phi_a u(\vec{x})$ and $\phi_v u(\vec{x})$ are generated such that they have an expected correlation of -0.8, but for the realization giving our "true" fields the correlation is actually higher.)

While working with the EnKF we generate an initial ensemble of size 200 of fields ϕ_a, ϕ_v and ϕ_{av} using the same construction as for the true field, but with the additional ϕ_v is truncated such that $\phi_v + \phi_a < 0.199$. The condition $\phi_v + \phi_a + \phi_{av} = 0.2$ corresponds to having full knowledge of CBV from the CAC data. While generating the initial ensemble we added a constraint that

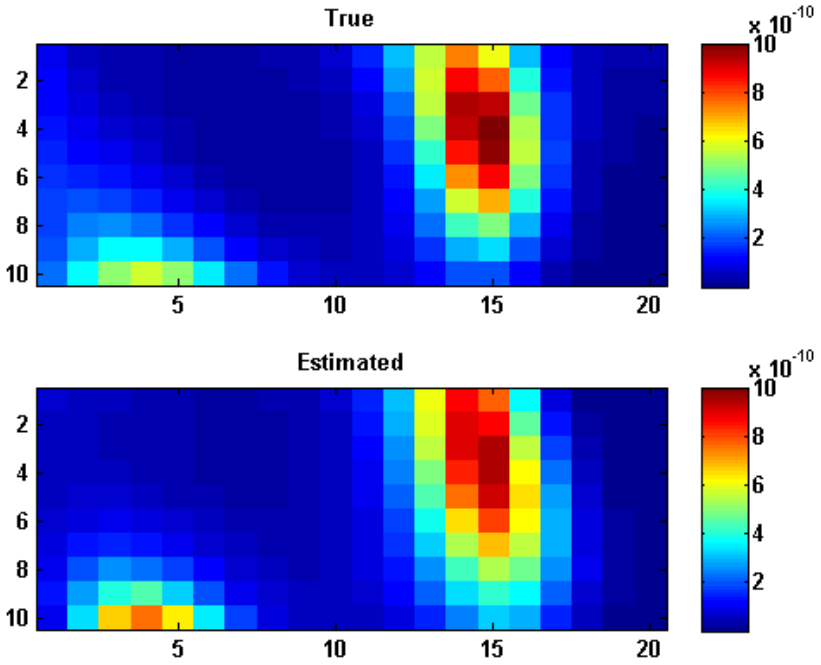

Figure 3: True permeability field (top) and mean value of estimated fields (bottom). The units are [m^{-2}].

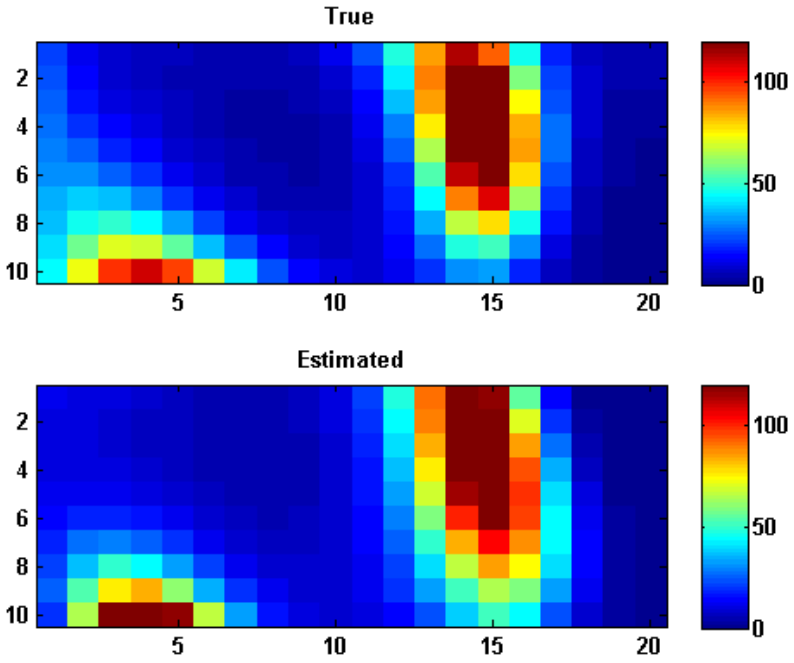

Figure 4: Estimated perfusion - CBF in units [mL/min/100mL].

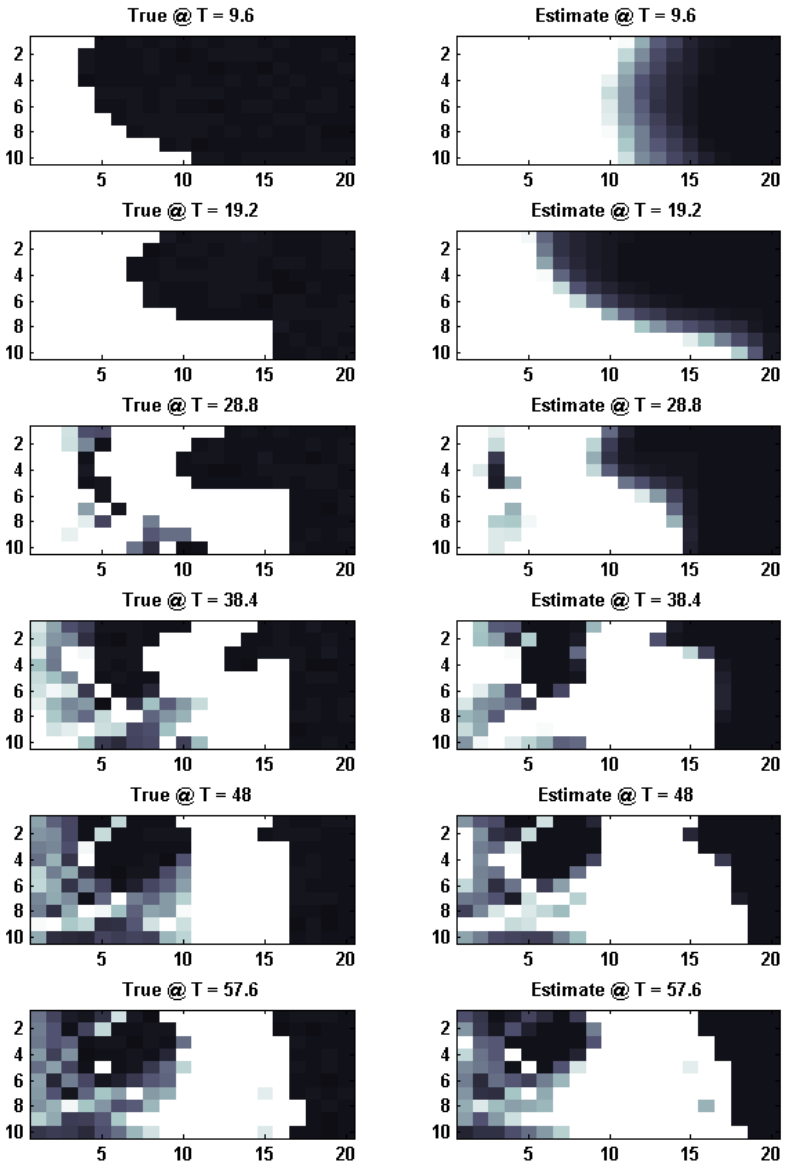

Figure 5: Simulated MRI data. Black indicate low intensity and white indicate high intensity. The range is between 0 and 10^{-2}.

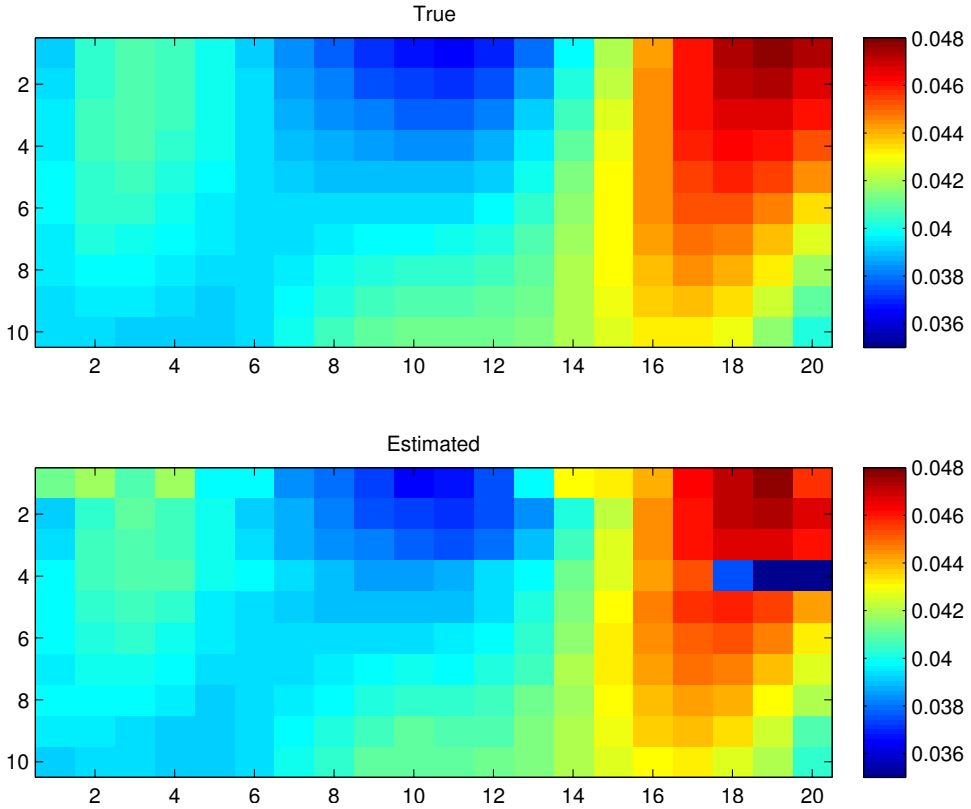

Figure 6: True and estimated ϕ_a.

all the porosity values always should be above 0.001. In the cases when the EnKF update step adjusted them below this value, they were truncated.

We observe the CAC for every 0.6 seconds for one minute with same type of measurement noise as in the previous example. This give a very large data set to assimilate. For the EnKF this poses additional challenges to avoid ensemble collapse. Therefore we restrict the use of each CAC observation to only update the porosities in its own location. Similar type of localization was used in [16] for updating a petroleum reservoir model using a seismic data set. The final estimates are shown in Figures 6 (bottom), 7 (bottom) and 8 (bottom). We note that the match all over is exceedingly good, except for a few locations. To avoid some extreme values to flatten the colors of the image, we have truncated the fields. For $\phi_v(\vec{x})$ there are two values above 0.16, the highest one 0.22. For $\phi_{av}(\vec{x})$ there are two locations having a value above 0.02, the highest one is 0.068. For four locations we came below 0.01, the lowest value was 0.001 (the truncation value). For $\phi_a(\vec{x})$ we got two values below 0.036, the lowest one was 0.001. The extreme values should be easily identified in the figures.

5 SUMMARY AND CONCLUSIONS

A two-compartment model is built with the aim of studying blood flow in live tissue. In a couple of synthetic examples we show that estimating important parameters as porosities of the compartments and the permeability seems feasible. In further studies, we need to generalize the estimation methodology to estimate these parameters jointly. In further studies there is also a clear need to proceed towards more realism in the biological modeling.

There are several issues that has been simplified in the modelling. The boundary condition is now assumed known, but in reality there will be uncertainty associated with it. Dispersion

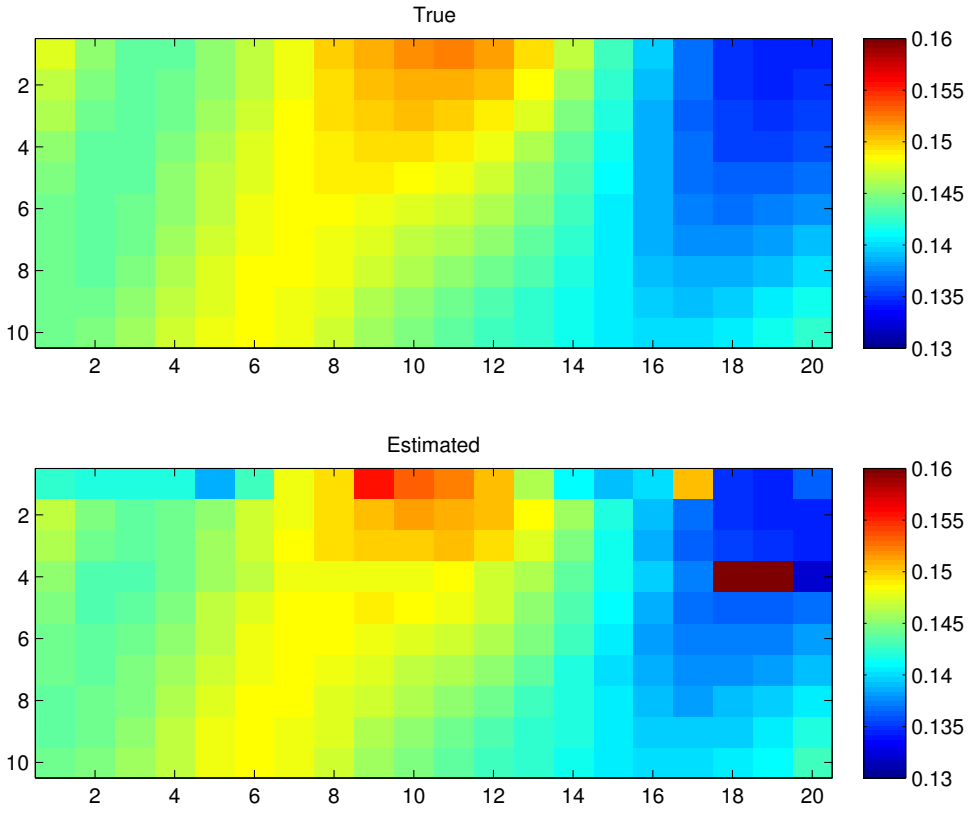

Figure 7: True and estimated ϕ_v.

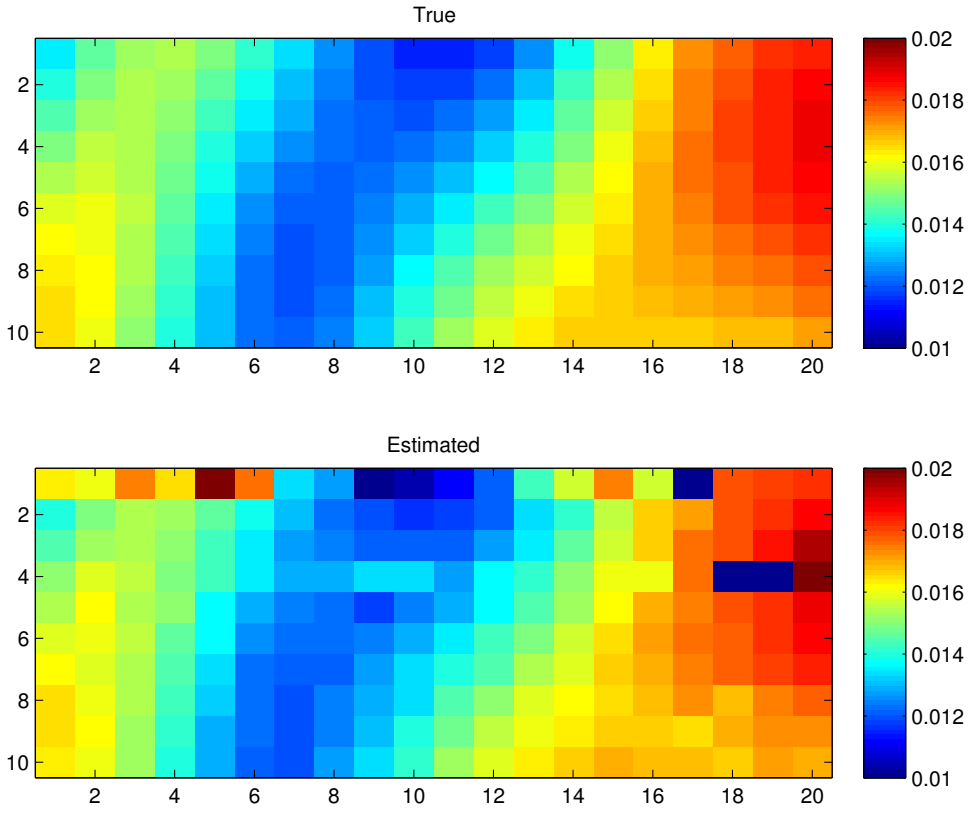

Figure 8: True and estimated ϕ_{av}.

effects are ignored, as well as the fact that the tissue will be in constant movement due to the heart pulse. However, while interpreting MRI images, any internal movement of the body has to be adjusted for to compare images at different time instances. Another interesting feature that might be added is the modelling is accounting for defects in the blood-brain barrier.

Both the EnKF and AGM that is used for data assimilation here, requires an initial ensemble based on a prior model. In the examples presented here, both the true model and the initial ensemble has been built based on the authors prior experience within geoscience. For modelling flow in live tissue, the prior assumptions need to be developed based on understanding of the biology of the actual system.

REFERENCES

[1] A. Fieselmann, M. Kowarschick, A. Ganguly, J. Hornegger, and R. Fahrig, Deconvolution-based CT and MR brain perfusion measurement: theoretical model revisited and practical implementation details. *International Journal of Biomedical Imaging*, **2011**, 20 pages, 2011.

[2] S. Sourbron, A tracer-kinetic field theory for medical imaging. *IEEE Transactions on Medical Imaging*, **33**, 4, 935–946, Apr. 2014.

[3] G. Evensen, *Data Assimilation: The Ensemble Kalman Filter*. Springer, 2007.

[4] S. I. Aanonsen, G. Nævdal, D. S. Oliver, A. C. Reynolds, and B. Vallès, The ensemble Kalman filter in reservoir engineering – a review. *SPE Journal*, **14**, 3, 393–412, Sep. 2009.

[5] D. S. Oliver and Y. Chen, Recent progress on reservoir history matching: a review. *Computational Geosciences*, **15**, 185–221, 2010.

[6] A. S. Stordal, H. A. Karlsen, G. Nævdal, H. J. Skaug, and B. Vallès, Bridging the ensemble Kalman filter and particle filters: the adaptive Gaussian mixture filter. *Computational Geosciences*, **15**, 2, 293–305, 2011.

[7] M. Ehrendorfer, A review of issues in ensemble-based Kalman filtering. *Meteorologische Zeitschrift*, **16**, 6, 795–818, Dec. 2007.

[8] F. Counillon, I. Bethke, N. Keenlyside, M. Bentsen, L. Bertino, and F. Zheng, Seasonal-to-decadal predictions with the ensemble Kalman filter and the Norwegian Earth System Model: a twin experiment. *Tellus A*, **66**, 21074, 2014.

[9] E. J. Kostelich, Y. Kuang, J. M. McDaniel, N. Z. Moore, N. L. Martirosyan, and M. C. Preul, Accurate state estimation from uncertain data and models: an application of data assimilation to mathematical models of human brain tumors. *Biology Direct*, **6**, 64, 2011.

[10] T. E. Yankeelov, V. Quaranta, K. J. Evans, and E. C. Rericha, Toward a science of tumor forecasting for clinical oncology. *Cancer Research*, **75**, 6, 918–923, Mar. 2015.

[11] S. Sourbron, M. Ingrisch, A. Siefert, M. Reiser, and K. Herrmann, Quantification of cerebral blood flow, cerebral blood volume, and blood-brain-barrier leakage with DCE-MRI. *Magnetic Resonance in Medicine*, **62**, 1, 205–217, 2009.

[12] R. E. Kalman, A new approach to linear filtering and prediction problems. *Transactions of the AMSE, Journal of Basic Engineering (Series D)*, **82**, 34–45, 1960.

[13] G. Evensen, Sequential data assimilation with a nonlinear quasi-geostrophic model using Monte Carlo methods to forecast error statistics. *J. Geophys. Res.*, **99**, C5, 10, 143–10, 162, 1994.

[14] A. S. Stordal, R. Valestrand, H. A. Karlsen, G. Nævdal, and H. J. Skaug, Comparing the adaptive Gaussian mixture filter with the ensemble Kalman filter on synthetic reservoir models. *Computational Geosciences*, **16**, 2, 467–482, Mar. 2012.

[15] N. Remy, A. Boucher, and J. Wu, *Applied Geostatistics with SGeMS*. Cambridge University Press, 2009.

[16] Y. Dong, Y. Gu, and D. S. Oliver, Sequential assimilation of 4D seismic data for reservoir description using the ensemble Kalman filter. *Journal of Petroleum Science and Engineering*, **53**, 83–99, 2006.